Journal of Engineering Physics and Thermophysics, Vol. 70, No. 2, 1997

EXPERIMENTAL AND THEORETICAL INVESTIGATION OF TAYLOR–GÖRTLER INSTABILITY IN THE BOUNDARY LAYER ON A CONCAVE SURFACE

A. A. Avramenko, S. G. Kobzar', and A. A. Khalatov

UDC 532.526

Results of experimental and theoretical investigations of centrifugal instability in the turbulent boundary layer on a concave surface are presented. Linear and nonlinear regularities in the development of this type of instability are revealed.

Concave surfaces are rather widespread in power engineering equipment, aerospace technology, etc. As a result of the active effect of centrifugal forces, longitudinal Taylor–Görtler macrovortices with an alternating direction of rotation are created in the vicinity of these surfaces. Up to now, mainly laminar Taylor–Görtler vortices have been studied. However, as has been shown by Tani's experiments [1], ordered macrostructures of this type also exist in turbulent flow. In recent years, more and more attention has been paid to this type of flow, since longitudinal macrovortices affect not only heat and momentum transfer processes but also resistance to vibration and hysteresis phenomena with variation of the Reynolds number, which are characteristic of exit diffusors of turbomachines [2].

Taylor–Görtler vortices have been investigated experimentally in [3, 4] and theoretically in a linear formulation in [5-8].

The present work is devoted to both experimental and theoretical investigations (in a linear formulation) of longitudinal macrovortices in a turbulent boundary layer.

Experiments were carried out on an open-type gas-dynamic contour. In order to eliminate perturbations at the entrance of the experimental section, which could affect the formation of Taylor–Görtler vortices, the fan for moving the working medium (air) operated in the pulling mode, i.e., was installed behind the experimental section. The experimental section consisted of two concentric surfaces (the working concave surface had radius $R_w = 120$ cm and a length of 70 cm) with a 10-cm gap between them. The transverse width of the working surface was 20 cm. A shutter was installed behind the working section to control the flow rate. Preswitched sections were installed forward of the experimental section to obtain various thicknesses of the boundary layer.

Experimental investigations were carried out using two methods: a method based on surface visualization and measurements with a constant-temperature thermoanemometer. The error of thermoanemometric measurements was 4.4%. Surface visualization was carried out using a naphthalene-saturated alcohol solution, which was sprayed on the concave surface. In the presence of vortices the film is carried away faster and, as time elapses, sharp longitudinal bands appear.

The experiments started with visual inspection of longitudinal macrovortices. It should be noted that the flow parameters (velocity at the external surface of the boundary layer u_∞ and thickness δ) were varied, taking into account the flow temperature, such that the Görtler number $\text{Gö} = u_\infty \delta / \nu K^{0.5}$ was in the region of linear instability, i.e., $\text{Gö} > \text{Gö}_{cr}$, where Gö_{cr} is the critical Görtler number calculated from linear stability theory [8]. Experiments have shown that, starting with a certain distance from the entrance to the working section, pronounced longitudinal bands appear, which can be interpreted as the presence of longitudinal Taylor–Görtler vortices. These bands diverge and broaden, which indicates an increase in the vortex wavelength (λ) downstream.

Institute of Technical Thermophysics of the National Academy of Sciences of Ukraine, Kiev, Ukraine.
Translated from Inzhenerno-Fizicheskii Zhurnal, Vol. 70, No. 2, pp. 279-283, March-April, 1997. Original article submitted November 28, 1994.

1062-0125/97/7002-0278$18.00

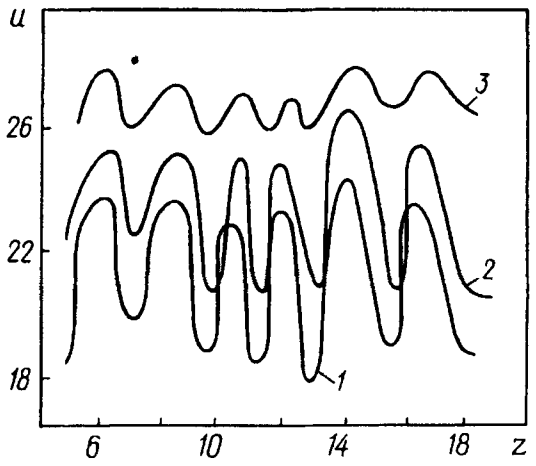

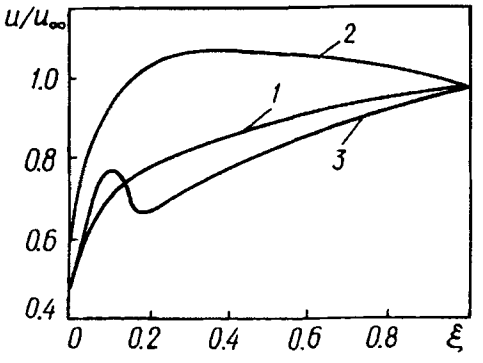

Fig. 1. Isotachs in boundary layer: 1) y = 5 mm, 2) 10, 3) 25. u, m/sec; z, cm.

Fig. 2. Velocity profiles in the boundary layer (z = var): 1) theoretical profile, 2) descending flow, 3) ascending flow.

However, as was shown by the thermoanemometric measurements, the vortex wavelength increases, so that the dimensionless quantity λ/δ remains virtually constant. Therefore, the dimensionless vortex wavenumber $\bar{\sigma} = \sigma\delta$, where $\sigma = 2\pi/\lambda$ is also a constant.

We have observed another interesting fact. A cardboard strip glued to the working surface leads to local separation of the boundary layer. As has been shown by both visualization and thermometric measurements, the vortices collapse in this case. At a certain distance, after boundary-layer reattachment, vortices appeared again. This type of flow development agrees with the data of [2], in which longitudinal vortices were generated by special insets in a curvilinear diffusor and collapsed during flow escape.

The results of thermoanemometric measurements for one transverse cross-section (x = const, where x is the curvilinear coordinate along the surface) are shown in Fig. 1. It is evident that the velocity in the plane y = const (y is the coordinate along the normal to the surface) varies periodically (quasiharmonically) in the transverse direction (along the z coordinate). Maximum relative oscillations were observed in the region $\xi = y/\delta$ = 0.3...0.4. When approaching the outer boundary, the isotachs become more straight. This is evidence of the fact that maximum perturbing velocities lie in the region ξ = 0.3 ... 0.4. In the region of the existence of vortices, the amplitude of velocity oscillations is virtually constant downstream. Therefore, we can conclude that the intensity of the vortex flow remains constant along the flow. As has been shown by measurements, the vortices are rather stable, although their positions oscillate somewhat about their axes. The period of vibrations is about 5 sec, and their amplitude is 4...5 mm, irrespective of the flow parameters. Velocity maxima on isotachs (Fig. 1) correspond to descending flows in the vortex. Thus, in this cross-section (z = const) the velocity profile is more filled. In the cross-sections in which isotachs have minima, ascending flows exist. Here the profile is filled to the maximum extent. Figure 2 shows velocity profiles in the boundary layer at z = var. Here we also present a calculated profile obtained numerically based on the Sebishi–Bradshaw model with allowance for the effect of surface curvature on turbulent viscosity [9]

$$\nu_t = \nu_{t0}\,(1 + \beta\,\mathrm{Ri})^2, \tag{1}$$

where ν_t and ν_{t0} are the turbulent viscosities of curvilinear and linear flows, respectively; $\mathrm{Ri} = 2\bar{u}/(R_w(\partial\bar{u}/\partial y))$ is the Richardson number;

$$\beta = 6.6274 - 7.843\left(\frac{\delta^{**}}{R_w}\cdot 10^3\right)^{0.143}.$$

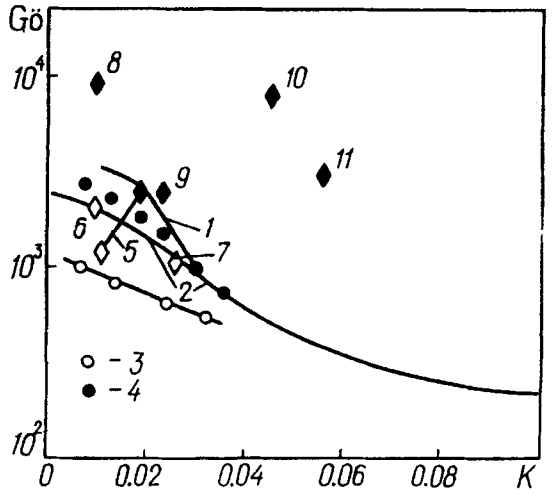

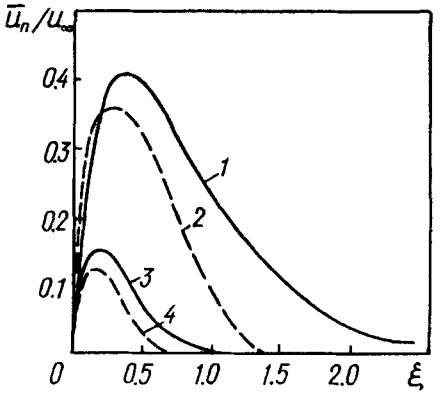

Fig. 3. Stability diagram: 1) calculation based on linear approximation; 2) calculation based on nonlinear approximation (3), 3) boundary of emergence of unstable vortices, 4) line of emergence of stable vortices, 5) line of emergence of vortices [3], 6) Shivaprasad–Ramaprian, 7) Toman, 8) Hofmann et al., 9) Meroni–Bradshaw, 10) Mail et al., 11) Jeens–Johns, vortices present (open diamonds), vortices absent (filled diamonds).

Fig. 4. Profiles of perturbing velocity amplitudes: 1, 3) theory (linear (4) and nonlinear (5), respectively), 2, 4) experiment (linear and nonlinear, respectively).

Then we attempted to determine the criterion for theemergence of vortices, i.e., criteria for centrifugal instability. Since the reproducibility of the vortices in numerous experiments was good, we decided to obtain a criterion for the emergence of Taylor–Görtler vortices by gradual increasing the flow rate or, which is the same, the Görtler number. This made it possible to show that, on reaching certain values of the Görtler number, spontaneously forming and decaying instable vortex structures emerge. A similar pattern has been observed in experiments [10]. Values of the Görtler number corresponding to this regime are shown in Fig. 3. It is evident that these Görtler numbers decrease with an increase in the curvature parameter K (in the region under investigation).

With a further increase in Gö, stable vortices emerged at a certain instant. These numbers are also shown in Fig. 3. The instant of emergence of these vortices is rather distinct. Therefore, in terms of [14], Taylor –Görtler turbulent instability can be called "strong," which is generally characteristic of various types of the centrifugal instability [12], and the Taylor perturbation method is the most suitable for theoretical investigations. The essence of the method consists in imposing the following perturbations on the main flow:

$$u = u_{up} + \sum_{n=0}^{\infty} u_n(y)\cos(n\sigma z)\exp(\gamma_n x),$$

$$v = v_{up} + \sum_{n=0}^{\infty} v_n(y)\cos(n\sigma z)\exp(\gamma_n x), \qquad (2)$$

$$w = \sum_{n=0}^{\infty} w_n(y)\sin(n\sigma z)\exp(\gamma_n x),$$

$$p = p_{up} + \sum_{n=0}^{\infty} p_n(y)\cos(n\sigma z)\exp(\gamma_n x).$$

We substitute these expressions into the equations of motion and, by equating terms of the sines and cosines with the same arguments, obtain an infinite system of equations. In order to determine theoretically criteria for the

emergence of Taylor–Görtler vortices, we must test the given system of equations for eigenvalues at $\gamma_n = 0$. When all harmonics except for the first ($n = 1$) are neglected, we arrive at a linear approximation [8, 13].

Two methods were used to investigate the obtained systems of equations. The first [14] is based on representation of the differential equations by their finite-difference analogs and subsequent evaluation of the determinant of the resulting system of algebraic equations at fixed values of all parameters entering the equation ($\mathrm{Re} = u_\infty \delta / \nu$, K, and $\bar{\sigma}$) except for one. When the determinant equals zero, we obtain eigenvalues of the system under investigation in the form of the dependence $\mathrm{G\ddot{o}} = \mathrm{G\ddot{o}}(\bar{\sigma})$. The minimum of this dependence is a criterion for the emergence of Taylor–Görtler vortices $\mathrm{G\ddot{o}}_{cr}$.

In the second case, the target method was used. Equations for perturbing amplitudes were solved by a numerical time-dependent method [15] with a single free parameter and a zero boundary condition. The missing boundary condition was replaced by a condition on the wall or external boundary of the boundary layer ($\xi = 1$) $dv_n/d\xi = 0$. The equations were solved repeatedly with subsequent correction of the free parameter in each step, until the free boundary condition was satisfied with the desired accuracy.

Both of the methods yield close results. The $\mathrm{G\ddot{o}}_{cr}$ values obtained in the linear approximation (only equations with $n = 1$ were taken into account) are presented in Fig. 3 (curve 1) as a function of the curvature parameter. A corresponding approximate dependence is presented in [8]. In the same figure, curve 2 was obtained within a nonlinear approximation for $n = 0, 1, 2$. Beginning with $n = 3$, allowance for higher-order approximations does not affect the results. Curve 2 can be approximated by the following dependence:

$$\mathrm{G\ddot{o}}_{cr} = \begin{cases} 2451 - 51{,}405\,K \quad \text{for} \quad K = 0, \ldots, 0.03\,, \\ 21.783\,K^{-1} - 0.2617\,K^{-2} + 5.784 \cdot 10^{-3} K^{-3} + 2.104 \cdot 10^{-4} K^{-4} \\ \text{for} \quad K = 0.03, \ldots, 0.1\,. \end{cases} \tag{3}$$

We used turbulence model (1) to obtain both curves. As is evident from Fig. 3, allowance for nonlinearity no longer affects the results of calculations for $K > 0.03$. The experimental data obtained in the present investigation lie closer to the nonlinear curve. In addition to eigenvalues of the equations under investigation, in solving the equations we obtained eigenfunctions representing the perturbation amplitudes, the maximum of which was the amplitude of the longitudinal velocity. Calculations show that the linear component $\bar{u}_1$ is virtually self-similar with respect to an incremental increase in perturbations, except for the region immediately adjacent to the surface, and is described by the expression

$$\bar{u}_1 = \frac{u_1}{u_\infty} = \begin{cases} 0.147\,\mathrm{G\ddot{o}}^{0.5}\xi & \text{when} \quad \xi \to 0\,, \\ S\xi \exp(-b\xi) & \text{when} \quad \xi > 0.01\,, \end{cases} \tag{4}$$

where $b \simeq 2.5$ and S is a weak function of curvature [8]. Profile (4) is shown in Fig. 4 along with experimental data from the profile of the total velocity (Fig. 2) with allowance for the theoretical profile (curve 1 in Fig. 2) and for the nonlinear component ($n = 0$). It is evident that the experimental profile has a somewhat lower maximum compared to the calculated profile (3), and the position of the maximum lies closer to the surface, so that $b \simeq 0.33$. The nonlinear component is also presented in Fig. 4. It is evident that it is much smaller than the linear component and has a maximum near the surface. In addition, a much sharper decay of the component is observed with increasing ξ.

In theoretical calculations of the nonlinear velocity component we decided to consider the amplitudes in formulas (2) to be functions of y and x in order to avoid introducing such an indefinite quantity as an incremental increase in perturbations γ_n. As a result, the following equation was derived for $\bar{u}_0 = u_0/u_\infty$:

$$\frac{d^2\bar{u}_0}{d\xi^2} + \frac{d\bar{u}_0}{d\xi}\left[\xi^{-1} + \xi^{1/n}\left(\frac{d\delta}{dx} + \frac{m}{m+1}\,\frac{d(u_\infty\delta)}{dx}\right)\frac{1}{\kappa}\sqrt{\left(\frac{2}{c_f}\right)}\right] +$$

$$+\frac{1}{\kappa}\sqrt{\left(\frac{2}{c_f}\right)}\,\xi^{(1-m)/m}\left(-\frac{\delta}{u_\infty}\frac{du_\infty}{dx}+\frac{1}{m}\frac{d\delta}{dx}\right)=-\frac{1}{2}u_1\frac{d\bar{u}_1}{dx}\frac{d\delta}{dx}\kappa\sqrt{\left(\frac{2}{c_f}\right)},$$

where m is the exponent in the power law of the distribution of the average velocity $u/u_1 = \xi^{1/m}$. The Galerkin method was used to solve the equation obtained with the coordinate functions chosen as follows:

$$\bar{u}_0 = \exp(-2b\xi)\sum_{k=1}^{\infty} a_k \xi^k. \tag{5}$$

Solution showed that the coefficient

$$a_1 = \frac{9}{4}\frac{S^2}{b\left(1-\frac{1}{m}\right)}$$

is the highest. The other coefficients are far behind in their absolute values. Profile (5) is presented in Fig. 4. It is evident that the theoretical profile agrees satisfactorily with the experimental one.

Thus, our investigations made it possible to reveal the presence of both linear and nonlinear phenomena in turbulent Taylor–Görtler vortices.

The work was supported by the State Foundation for Basic Research of the State Committee on Science and Technologies of Ukraine.

NOTATION

ν, kinematic viscosity; δ, thickness of the boundary layer; u_∞, velocity on the external surface of the boundary layer; R_w, curvature radius of the surface; $K = \delta/R_w$, curvature parameter; λ, vortex wavelength; σ, wavenumber; x, y, z, curvilinear orthogonal coordinates; $\xi = y/\delta$; u, v, w, velocity components along coordinates x, y, and z; p, pressure; γ_n, incremental increase in perturbations; $\kappa = 0.4$, Carman's constant; $c_f = 2\tau_w/(\rho u_\infty^2)$, friction coefficient; τ_w, surface friction; ρ, desnity; n, number of perturbing harmonic. Subscripts and superscripts: up, unperturbed quantities; cr, critical value; f, friction; w, wall.

REFERENCES

1. I. Tani, Geophys. Res., 67, No. 8, 3075-3080 (1962).
2. L. M.Genka, R. L. Panton, and D. G. Bogchard, Sovr. Mashinostr. [Russian translation], Ser. A, No. 12, 118-125 (1989).
3. J. Kim, T. W. Simon, and S. G. Russ, J. Heat Transfer, **114**, No. 2, 338-347 (1992).
4. M. D. Kestoras and T. W. Simon, J. Turbomachinery, **114**, No. 4, 891-898 (1992).
5. R. Kobayashi and N. Fujisawa, J. Appl. Mech., **47**, No. 3, 671-672 (1980).
6. N. Fujisawa, R. Kobayashi, and H. Shirai, J. Appl. Mech., **52**, No. 2, 492-493 (1985).
7. N. Fujisawa and H. Shirai, Bull. JSME, **29**, No. 257, 3761-3766 (1986).
8. A. A. Khalatov and A. A. Avramenko, Teplofiz. Vys. Temp., **32**, No. 1, 69-71 (1994).
9. A. A. Khalatov, A. A. Avramenko, and I. V. Shevchuk, Heat Transfer and Hydrodynamics Near Curvilinear Surfaces [in Russian], Kiev (1992).
10. R. S. Barlow and J. P. Johnston, J. Fluid Mech., **191**, 177-196 (1988).
11. G. Z. Gershuni and E. M. Zhukhovitskii, Convective Stability of Incompressible Fluid [in Russian], Moscow (1972).
12. W. L. Hung, D. D. Joseph, and B. R. Munson, J. Fluid Mech., **51**, 593-624 (1972).
13. A. A. Avramenko and A. A. Khalatov, Promyshl. Teplotekhn., **15**, 29-33 (1993).
14. L. Kollatus, Eigenvalue Problems [Russian translation], Moscow (1968).
15. K. Fletcher, Computational Methods in Fluid Dynamics [Russian translation], Moscow (1981).